EPJ Web of Conferences **233**, 05005 (2020) https://doi.org/10.1051/epjconf/202023305005
CMPNC 2019

Orthorhombic $GdMnO_3$ Epitaxial Thin Film Grown onto SrTiO3 (110)

P. Machado[1], F. G. Figueiras[1], R. Vilarinho[1], J. R. A. Fernandes[2], P. B. Tavares[3], M. Rosário Soares[4], S. Cardoso[5], A. Almeida[1], J. Agostinho Moreira[1]

[1]IFIMUP e Departamento de Física e Astronomia, Faculdade de Ciências da Universidade do Porto. R. Campo Alegre 687, 4169-007 Porto, Portugal
[2]CQVR e Departamento de Física, Universidade de Trás-os-Montes e Alto-Douro, Ap.º 1013, 5001-801 Vila Real, Portugal
[3]CQVR e Departamento de Química, Universidade de Trás-os-Montes e Alto-Douro, Ap.º 1013, 5001-801 Vila Real, Portugal
[4]CICECO & LCA, Universidade de Aveiro, 3810-193 Aveiro, Portugal
[5]INESC-MN, Rua Alves Redol, 9, 1000-029 Lisboa, Portugal

Abstract. $GdMnO_3$ epitaxial thin films were deposited onto (110)-oriented $SrTiO_3$ substrates by RF magnetron sputtering. The structure, microstructure, dielectric and magnetic properties were investigated in detail. The XRD results revealed that the $GdMnO_3$ thin films exhibit an epitaxial strained orthorhombic symmetry and grow preferably in off-plane (001) orientation, wherein the basal lattice parameters are strained by the substrate lattice. A dielectric relaxation process was ascertained, whose activation energy is sensitive to the magnetic phase transitions, occurring at 41 K and at 20 K, respectively. The canted nature of the low temperature magnetic phase is discussed.

1 Introduction

The demand for new materials with higher performance and versatility has been focused on those exhibiting coupling between different degrees of freedom [1,2]. The knowledge concerning the microscopic mechanisms underlying the coupling between orbital, electronic, spin and lattice degrees of freedom, occurring in transition metal oxides with perovskite structure, has been able to advance in the design of new multifunctional materials. In this regard, the rare-earth orthomanganites ($RMnO_3$) with P*nma* symmetry have been deeply studied as their physical properties are very sensitive to structure due to the spin-orbital-lattice coupling [3,4]. It was established, both experimentally and theoretically, that the interesting magnetic and ferroelectric (multiferroic) properties found for some $RMnO_3$ are constrained by the Mn-O-Mn bond angle [4,5]. Changing the Mn-O-Mn bond angle, the orbital overlap between adjacent Mn^{3+} and O^{2-} ions is altered, which consequently modifies the magnetic superexchange integrals between the magnetic Mn^{3+} ions, crucial for the stabilization of the different spin arrangements [5].

$GdMnO_3$ (GMO) stands at the border between the non-multiferroic and multiferroic regions of the phase diagram of $RMnO_3$ [3,5]. On cooling, GMO undergoes a transition into a collinear-sinusoidal incommensurate antiferromagnetic (AFM) at T_N = 43 K and then a

transition to a canted A-type AFM phase at T_c = 22 K, both associated with the Mn^{3+} spins [3,5]. The long range order of Gd^{3+} magnetic moments emerges below T_N'= 6.5K [3]. Multiferroicity can be achieved below T_C by applying a magnetic-field above 2 T, wherein a magnetically-order ferroelectric phase emerges via magnetoelectric coupling [6]. Spontaneous ferroelectricity can also be obtained by slightly reducing the Mn-O-Mn bond angle via chemical substitution of the Gd^{3+} ions by Tb^{3+}, Y^{3+}, among others [7,8]. The interplay between structure and magnetism can be changed using structural distortions. Here we highlight that ferroelectricity was achieved below 30 and 75 K on orthorhombic GMO thin-films with 10 and 110 nm, deposited by pulsed laser deposition onto (010)-$YAlO_3$ and (001)-$SrTiO_3$ substrates, respectively [9,10]. Recently, the study of epitaxially strained GMO thin-films deposited on (001)-$SrTiO_3$ substrate by RF magnetron sputtering, conveyed an unprecedently reported tetragonal structure at room temperature and ferroelectric below 32 K, up to 35 nm thick films [11]. The emergence of a spontaneous electric polarization in these films reveal the stabilization of a low temperature improper ferroelectric phase, not observed in bulk GMO. In order to go further in the study of the structure-related physical properties of GMO, we present a structural, magnetic and dielectric study of GMO thin-films deposited onto (110)-$SrTiO_3$ substrates through RF magnetron sputtering method. We aim at unravelling the role played by the crystallographic orientation of the substrate onto the film structure and its physical properties. The results obtained will be examined in detail, and compared with those reported for identically deposited GMO thin-films, though grown on (001)-$SrTiO_3$ substrates.

2 Experimental Details

GMO polycrystalline targets were prepared following the procedure described elsewhere [11]. Polished (110)-oriented $SrTiO_3$ substrates (STO(110)) were previously cleaned before deposition in ultrasonic baths and dried using N_2 flow. GMO thin films were deposited onto STO(110) at 800 °C, through RF-magnetron sputtering, working at 13.56 MHz and 80 W RF power. The distance between target and substrate was 130 mm. The deposition rate was 2 nm/min. The pressure inside the chamber was adjusted to $5x10^{-2}$ mbar, with a gas composition setting a ratio of Ar:O_2 of 4:1. After deposition, the films were cooled naturally in a pure oxygen atmosphere of 1 mbar, without any annealing step. The crystallographic structure was measured by high resolution X-ray diffraction at room conditions, using a X'Pert MRD Philips four-circle diffractometer, in a Bragg–Brentano para-focusing configuration, operating with Cu Kα radiation at 30 mA and 40 kV, and analysed through the Le Bail mode. In-plane specific magnetization measurements were carried out using a SQUID magnetometer, with a resolution better than $5x10^{-7}$ emu. The complex electric permittivity was measured in the 1 kHz - 1 MHz frequency range with an HP4284A impedance analyser, under a 50 V/cm ac electric field [11]. 50 gold interdigital electrodes (IDEs), with 7 mm length, 20 μm width, 20 μm interspacing and depth of about 90% of the thickness of the deposited film, were used for the measurements [11].

3 Results and discussion

Figure 1(a) displays the X-ray Reflectometry diffractogram of GMO thin film onto STO(110) substrate exhibiting low contrast fringes, from which the thickness of 44 ± 4 nm can be estimated. Figure 1(b) presents the conventional X-ray diffraction pattern (red line). The main STO reflections are observed at 2Θ = 32.14°, 67.56°, assigned to (110) and (220) planes, respectively, confirming the (110)-orientation of the substrate and, ascribing a_{STO} = 3.91(0) Å, in good agreement to referenced data [9].

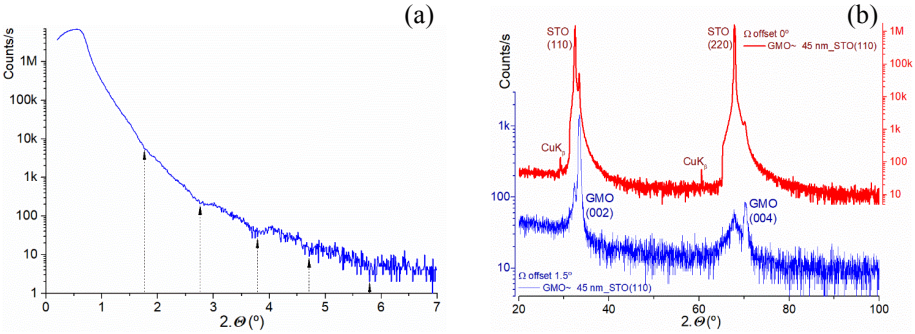

Fig. 1. Diffractograms of the 44 nm GMO/STO(110) thin film (a) XRR with respective fringes signalled by arrows, and (b) XRD pattern (red line) and using a $\Delta\Omega = 1.5°$ offset (blue line).

No evidences of spurious GdO_x or MnO_x phases were found. By adjusting the XRD acquisition parameters with a $\Delta\Omega = 1.5°$ offset (blue line in Figure 1(b)), it allows to focus on the GMO film layer and surpass substrate reflections. The main peaks at $2\Theta = 33.43°$ and 70.24° are assigned respectively to the (002) and (004) planes of the GMO phase, evidencing the preferential off-plane growth of GMO oriented along *c*-axis. In addition, it is possible to perceive a slight Bragg peak at $2\Theta = 31.25°$, indexed to the reflection on the (200) planes. This evidences that the films do not grow uniformly and two different GMO layers (hereafter called α- and γ-layers) are present.

Figure 2(a) shows the symmetric XRD space map in the Θ-Ω coordinates, at $2\Theta = 32.43°$ and $\Omega = 16.22°$, centred at the STO(110) reflection peak. This map evidences the presence of 3 reflection peaks emerging from the GMO thin film. The main peak found at $2\Theta = 33.35°$, with $\Omega = 16.72°$ shadows the shape of the STO(110) peak, and shows a long relaxation tail visible up to $2\Theta = 37°$, which can be associated with Laue interference fringes, typically found in a layered topology. This peak is consistent with the reflection on the GMO (002)-planes, confirming the off-plane growth direction along c_γ-axis, and yielding a lattice parameter $c_\gamma = 5.372(4)$ Å, assigned to the γ-layer. Two additional satellite peaks are observed at $2\Theta = 31.24°$, extending orthogonally to each side of STO(110) peak at $\Omega = 18.87°$ and $\Omega = 12.25°$. These peaks are indexed to GMO (200)-plane reflections. Although relatively faint, these two peaks are well-defined ($\Delta 2\Theta \sim \pm 0.5°$, $\Delta\Omega \sim \pm 0.5°$), thus evidencing the presence of a twined crystalline growth along a_α-axis in the off-plane direction, with a calculated lattice parameter $a_\alpha = 5.72(2)$ Å of the α-layer. The low ratio between the I_α/I_γ peaks intensity suggests the α-layer is only a few nanometres thick. The asymmetric space map over the reflection on GMO (114) planes, displayed in Figure 2(b), shows a regular single peak positioned at $2\Theta = 73.69°$, which does not point to any twinning effects, in good agreement with the rather small thickness of α-layer.

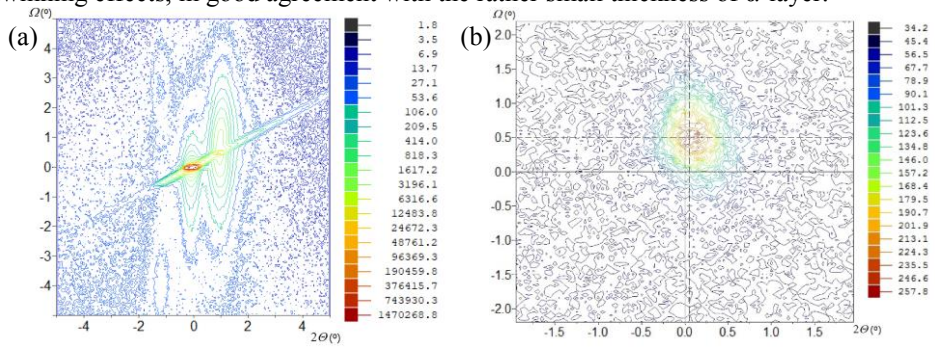

Fig. 2. (a) Symmetric Θ-Ω over substrate reflection (110) at $2\Theta = 32.42°$ and $\Omega = 16.21°$; (b) asymmetric (114) reflection at $2\Theta = 73.69°$, $\Omega = 19.78°$, $\Phi = 38.64°$ and $\Psi = -0.38°$ space maps.

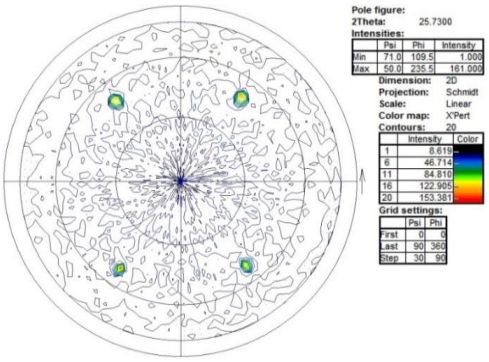

Fig. 3. Symmetric pole figure encompassing thin film (111) central reflection at 2Θ = 25.73°.

Table 1. Lattice parameters and relative variations of GMO thin film to STO substrate and bulk GMO.

STO substrate (Å)	$\Delta_{\gamma/STO}$ (%)	GMO γ-layer (Å)	$\Delta_{\gamma/GMO}$ (%)	GMO bulk (Å)
$\sqrt{2}.a_{STO}$ 5.530	< +1.4	a_γ 5.60(8)	< -4.4	a_o 5.866
$2.a_{STO}$ 7.820	> -2.3	b_γ 7.64(1)	> +2.8	b_o 7.431
		c_γ 5.37(2)	> +1.0	c_o 5.318
		V_γ 230.1(8)	< -0.7	V_o 231.81

Figure 3 shows the symmetric pole figure obtained at 2Θ = 25.73° corresponding to reflection on the (111) planes of the GMO film. The observation of 4 reflections near Ψ ~ 50.0° ± 0.1° positioned at Φ = 55.2°, 128.2°, 235.5° and 307.6°, confirms the orthorhombic symmetry of the GMO phase, and is compatible with the dominant off-plane preferential growth orientation of the film along c_γ-axis, from the γ-layer, with a_γ- and b_γ-axes being in-plane. The average projected angle ΔΦ = 36.3°± 0.2° corresponds to the relation a_γ/b_γ = 0.734(0). The calculated lattice parameters and the respective relative distortions to the STO substrate and bulk GMO are shown in Table 1, and appear as a compromise between both. Due to the reduced presence of α-layer, it was not possible to obtain the values of the in-plane b_α and c_α directly. Nonetheless, α-layer is highly constrained by epitaxial relations to either the STO(110) and the GMO γ-layer, corresponding to: $\sqrt{2}a_{STO} > c_\alpha \approx c_\gamma > c_0 > a_\gamma$, and to $2a_{STO} > b_\alpha \approx b_\gamma > b_o$, which forcibly leads to an expansion of the lattice volume relative to the bulk GMO, estimated between +1.3% minimum and +6.8% maximum. Since γ-layer volume has a less pronounced variation of -0.7% from the bulk GMO, it suggests that α-layer grows on the STO substrate and acts as buffer for γ-layer.

Figures 4(a) and (b) show the real and imaginary part of the complex dielectric permittivity as a function of temperature, in the 20 kHz to 1 MHz frequency range. As temperature decreases, for frequencies above 100 kHz, the ε'(T) curves increase and reach a maximum at a frequency dependent temperature, while for frequencies below to 100 kHz this maximum is not reached down to 10 K. The ε''(T) curves monotonously increase as temperature decreases, with a strongly frequency dependent slope. These frequency dependent features are a clear evidence for a relaxation process that hinders the direct observation of anomalies associated with phase transitions. Figure 4(c) shows the Cole-Cole plots at different temperatures, which follow well defined semicircles at low temperatures, becoming gradually shorter for higher temperatures. The relaxation frequency was taken at the maximum of each semicircles, to obtain the Arrhenius plot shown in Figure 4(d). The data cannot be described by a single linear regime for the whole range. Two changes of slope occur, one between 35 K and 45 K, and another at around 20 K, associated with changes of the relaxation process activation energy. Above 45 K, the relaxation process activation energy is 7.3 ± 0.4 meV, between 35-45 K and 20 K it reduces to 1.8 ± 0.2 meV, while below 20 K it further drops to 0.46 ± 0.03 meV. Similar changes of the activation energy were also observed in bulk GMO, though from values of 10 to 20 meV, having been correlated with magnetic phase transitions [12]. Thus, we expect to have two phase transitions, one between 35 and 45 K, and another around 20 K. These temperatures are close to the two critical temperatures found in bulk GMO.

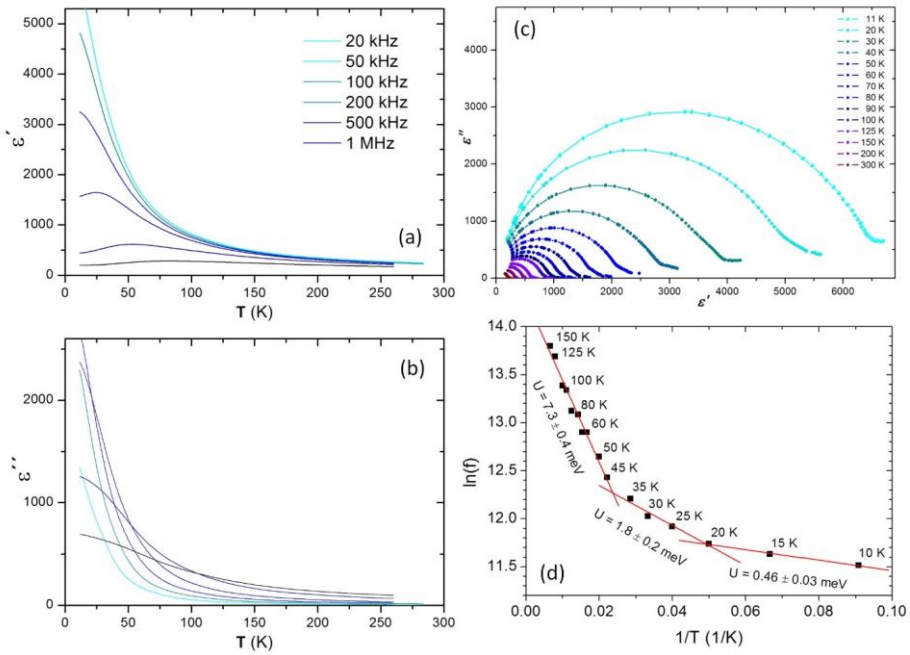

Fig. 4. (a) Real part and (b) imaginary part of complex dielectric permittivity measured in plane as a function of temperature for different fixed frequencies. (c) Cole-Cole plots at different fixed temperatures. (d) Arrhenius plot for the relaxation process with respective activation energies.

Figure 5 shows the magnetic response of the GMO film onto STO(110) substrate, measured in ZFC and FC conditions, under a 40 Oe magnetic field. The M(T) curve measured in ZFC conditions exhibits a peak-like anomaly at 20 K, at the same temperature where the change in the activation energy of the relaxation process is observed. The value of the M(T) increases significantly in FC conditions just below 25K. This result evidences for the stabilization of a canted AFM phase below T_C =20 K, which is responsible for the large increase of the separation between the ZFC and FC curves below this temperature. A faint but clear anomaly in M(T) measured in both ZFC and FC conditions is observed at 41 K, within the temperature interval of the second change in the activation energy. Although our data does not allow to unravel the nature of this anomaly, the stabilization of another magnetic phase cannot be excluded.

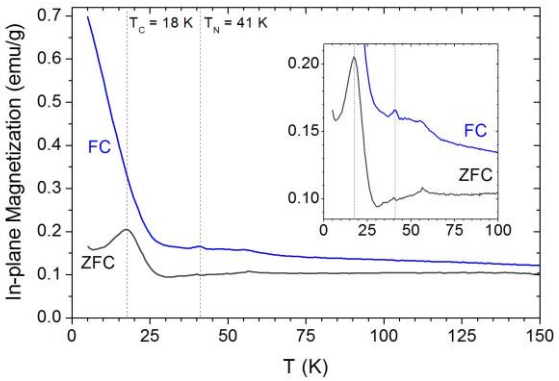

Fig. 5. In-plane magnetic response as a function of temperature, measured in ZFC and FC conditions with an applied field of 40 Oe. Vertical dashes lines mark phase transitions.

Although anomalies in the M(T) curves can also be seen at 55 K, we do not assign any magnetic phase transitions for two reasons: i) the relaxation process activation energy does not change at this temperature; ii) it has been reported that spurious oxygen found inside the SQUID magnetometer originates such type of anomalies around 55 K [13].

4 Conclusions

High quality GMO thin films were deposited onto (110)-oriented $SrTiO_3$ substrates by RF magnetron sputtering. The films exhibit an epitaxial orthorhombic symmetry, where the basal lattice parameters are strained by the cubic structure of the substrate, imposing a twinned α-phase on the GMO thin films in (100) direction that evolves to a γ-phase that grows preferably in (001) orientation. Both phases of the orthorhombic GMO thin film grown on STO(110) exhibit lattice parameters considerably less distorted in relation to the GMO bulk form than the tetragonal GMO thin film grown on STO(001). On the other hand, the volume compression of both the tetragonal and the main orthorhombic phases are noteworthy similar to -0.7% which denotes that this compression value is energetically favourable to the GMO perovskite phase under epitaxial strain. The temperature dependence of the relaxation process activation energy suggests for the existence of two magnetic phase transitions, also marked by anomalies in the M(T) curves. The magnetization data give clear evidence a canted AFM phase below Tc = 20 K.

References

1 W. Eerenstein, N.D. Mathur, J.F. Scott, Nature **442**, 759 (2006)

2 M. Bibes and A. Barthélémy, Nat. Mater. **7**, 426 (2008)

3 T. Kimura, T. Goto, H. Shintani, K. Ishizaka, T. Arima, Y. Tokura, Nature **426**, 55 (2003)

4 T. Kimura, S. Ishihara, H. Shintani, T. Arima, K.T. Takahashi, K. Ishizaka, and Y. Tokura, Phys. Rev. B **68**, 060403(R) (2003)

5 M. Mochizuki and N. Furukawa, Phys. Rev. B **80**, 134416 (2009)

6 T. Kimura, G. Lawes, T. Goto, Y. Tokura, A. Ramirez, Phys. Rev. B **71**, 224425 (2005)

7 T.Goto, Y.Yamasaki, H.Watanabe, T.Kimura, Y.Tokura, Phys. Rev. B **72**, 220403 (2005)

8 R. Vilarinho, A. Almeida, J.M. Machado da Silva, J.B. Oliveira, M.A. Sá, P.B. Tavares, J. Agostinho Moreira, Solid State Commun. **208**, 34 (2015)

9 X. Li, C. Lu, J. Dai, S. Dong, Y. Chen, N. Hu, G. Wu, M. Liu, Z. Yan, J.-M. Liu, Sci. Rep. **4**, 7019 (2014)

10 S. Mukherjee, K. Shimamoto, Y.W. Windsor, M. Ramakrishnan, S. Parchenko, U. Staub, L. Chapon, B. Ouladdiaf, M. Medarde, T. Shang, E.A. Müller, M. Kenzelmann, T. Lippert, C.W. Schneider, and. Niedermayer, Phys. Rev. B **98**, 174416 (2018)

11 P. Machado, F.G. Figueiras, R. Vilarinho, J.R.A. Fernandes, P.B. Tavares, M.R. Soares, S. Cardoso, J.P.B. Silva, A. Almeida, J.A. Moreira, Sci. Rep. accepted (2019)

12 R. Vilarinho, Magnetically-Induced Ferroelectricity Unraveled Through Spin-Phonon Coupling, University of Porto (2013)

13 D.G. Friend, NIST Stand. Ref. Databases volume 12 (1992)